Control over Charge Transfer through Molecular Wires by Temperature and Chemical Structure Modifications

ARTICLE *in* ACS NANO · OCTOBER 2010

Impact Factor: 12.88 · DOI: 10.1021/nn1013758 · Source: PubMed

Control over Charge Transfer through Molecular Wires by Temperature and Chemical Structure Modifications

Mateusz Wielopolski,[†] Gustavo de Miguel Rojas,[†] Cornelia van der Pol,[‡] Linda Brinkhaus,[†] Georgios Katsukis,[†] Martin R. Bryce,[‡,*] Timothy Clark,[§,*] and Dirk M. Guldi[†,*]

[†]Department of Chemistry and Pharmacy & Interdisciplinary Center for Molecular Materials, Friedrich-Alexander-Universität Erlangen-Nürnberg, Egerlandstr. 3, 91058 Erlangen, Germany, [‡]Department of Chemistry, Durham University, Durham DH1 3LE, United Kingdom, and [§]Department of Chemistry and Pharmacy & Interdisciplinary Center for Molecular Materials (ICMM), Computer Chemistry Center (CCC), Friedrich-Alexander-Universität Erlangen-Nürnberg, Nägelsbacherstrasse 25, 91052 Erlangen, Germany

ABSTRACT A series of electron donor–acceptor arrays containing π-conjugated oligofluorenes (oFL) of variable length between a zinc porphyrin (ZnP) as electron donor and fullerene (C_{60}) as electron acceptor have been prepared by following a convergent synthesis. The electronic interactions between the electroactive species were determined by cyclic voltammetry, UV–visible, fluorescence, and femto/nanosecond transient absorption spectroscopy. Our studies clearly confirm that, although the C_{60} units are connected to the ZnP donor through π-conjugated oFL frameworks, no significant electronic interactions prevail in the ground state. Theoretical calculations predict that a long-range electron transfer occurs primarily due to a maximized π-conjugated pathway from the donor to the acceptor. Photoexcitation of ZnP-oFL$_n$-C_{60} results in transient absorption maxima at 715 and 1010 nm, which are unambiguously attributed to the photolytically generated radical ion pair state, [ZnP$^{\bullet+}$-oFL$_n$-$C_{60}^{\bullet-}$], with lifetimes in the microsecond time regime. Temperature-dependent photophysical experiments have shown that the charge-transfer mechanism is controllable by temperature. Both charge separation and charge recombination processes give rise to a molecular wire behavior of the oFL moiety with an attenuation factor (β) of 0.097 Å^{-1}. The correlation β to the connection pattern between the ZnP donor and the oFL linker revealed that even small alterations of the linker π-electron system break the homogeneous π-conjugation pattern, leading to higher values of β.

KEYWORDS: molecular wires · electron donor–acceptor conjugates · cycloaddition reactions · charge transfer · transient absorption spectroscopy · temperature dependence · excited-state calculations · oligofluorenes · zinc porphyrins · fullerenes

The reason for the growing popularity of one-dimensional molecular wires is their potential for applications in sensors, optoelectronics, photovoltaics, and emerging nanoscale technologies.[1−3] The latter may easily be understood regarding photoinduced charge-transfer processes in electron donor–acceptor conjugates.[4−6] Many successful strategies have been developed to assess and control the magnitude of charge transfer through such conjugates. The function of the linker is the mediation of charges between two photo- and/or redox-active components, namely, the donor and the acceptor.[7] Linear π-conjugated oligomers with well-defined chemical structures are best suited as linking components in these conjugates.[8−10] Here, the systematic variation of parameters such as the redox potentials of the end groups, intramolecular distances (*i.e.*, length of the linker), topology, and relative orientations of the component units enables charge separation and storage characteristics to be probed in detail by electrochemical and spectroscopic techniques.

To assess charge transfer over long distances,[11] irradiation with light may cause photoinduced transport of charges from the donor to the acceptor. The rate of the charge separation processes is governed by parameters related to the properties of the donor and the acceptor, such as the driving force ($-\Delta G^0$), the reorganization energy (λ), and the electronic coupling (V), which are determined by both the structure of the bridge and the donor-bridge energy gap. The efficiency of the electron transfer (ET) decreases exponentially with increasing length of the linker moiety according to the electron-transfer rate constant, k_{ET}

$$k_{ET} = k_0 e^{-\beta R_{DA}} \qquad (1)$$

where k_0 is the kinetic prefactor, R_{DA} represents the donor–acceptor distance, and β is the attenuation factor, which depends on the intrinsic electronic properties of the linker.[12]

The attenuation factor β is also used to determine whether an electron donor–acceptor system should be considered to display wire-like behavior at all. Equation 1 predicts that a small β would allow charges to be transferred over larger distances. Importantly, such a definition of β applies only to exponentially decaying processes. In addition, the limit of very small β describes band transport, a so-called

*Address correspondence to guldi@chemie.uni-erlangen.de, m.r.bryce@durham.ac.uk, clark@chemie.uni-erlangen.de.

Received for review June 18, 2010 and accepted October 11, 2010.

Published online October 21, 2010. 10.1021/nn1013758

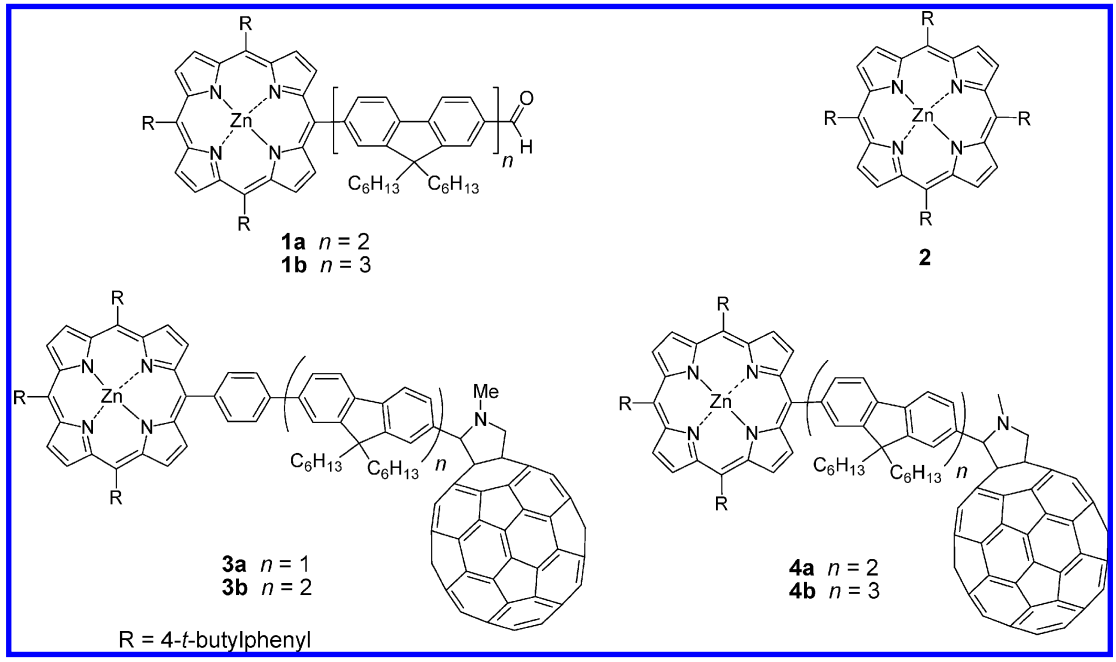

Figure 1. Structures of the ZnP-oFL$_n$-C$_{60}$ conjugates and their reference compounds.

"π-electron pathway", along which the electrons travel coherently.[13] Shallow distance dependence may also result from a series of short-range tunneling events. This is equivalent to incoherent hopping, which *per se* does not follow an exponential decay with increasing distance.[14−16]

Interestingly, β values for identical linkers vary significantly. The magnitude of β reflects, for example, the sensitivity of the transport process to the surrounding environment. Distance dependence is one of these parameters. Typical values for β range between 1.0 and 1.4 Å^{-1} for proteins[17] and between 0.001 and 0.06 Å^{-1} for highly efficient π-conjugated linkers.[18,19] Another key aspect for achieving efficient molecular wire behavior in electron donor−acceptor systems is the effective matching of orbital energies between the donor and the linker components and between the linker and acceptor components.[6,20] For example, for electron donor−acceptor systems incorporating extended tetrathiafulvalene donors (exTTF), oligo-*para*-phenylenevinylene (oPPV) linkers, and fullerene acceptors (exTTF-oPPV-C$_{60}$), extremely small β values (0.01 Å^{-1}) have been reported. Highly extended and homogeneous π-conjugation between exTTF, oPPV, and C$_{60}$ are responsible for an efficient electron transfer between donor and acceptor.[21,22] Upon exchanging the donor or the linker, an increase in the β value is observed due to a lower effective conjugation between the electroactive components. For oligo-*para*-phenyleneethynylenes (oPPE) in exTTF-oPPE-C$_{60}$ conjugates, for instance, an increased attenuation factor of 0.20 Å^{-1} has been obtained.[23,24] In photoinduced charge-transfer studies, free base (H$_2$P) or metalated zinc porphyrin (ZnP), H$_2$P-oPPE-C$_{60}$/ZnP-oPPE-C$_{60}$,[25] have shown β values of 0.11 Å^{-1} and exTTF-oFL-C$_{60}$[26,27] of 0.09 Å^{-1}. Interestingly, tetraphenylporphyrin (TPP) conjugates, TPP-oPPV-C$_{60}$,[28] exhibited values of β as low as 0.03 Å^{-1}, which are nonetheless larger than those of the corresponding exTTF analogues (*i.e.*, exTTF-oPPV-C$_{60}$).[21] This trend has been explained by dihedral angles of *ca.* 30° between the TPP phenyl ring and the first ring of the oligomer linker. Such a deviation from planarity breaks the highly effective *para*-conjugation pattern along the oligomer unit. Numerous other examples have been reported of molecular architectures formed by porphyrins and fullerenes linked by various groups, which exhibit efficient long-distance photoinduced electron transfer from the porphyrin to the fullerene.[29−34]

We now report on a novel series of ZnP-oFL-C$_{60}$ conjugates that incorporate ZnP as the donor and C$_{60}$ as the acceptor covalently linked by oligofluorene (oFL) units of variable length. In particular, this study focuses on modulating the kinetics of electron-transfer processes—the attenuation factor β—by distinctive temperature control[35] and the structural modification of the connection pattern between the linker and the donor. Specifically, the impact of incorporating an additional phenyl ring between the ZnP and the oFL moiety (Figure 1) on the charge transport properties of the linker will be elaborated. Does the additional phenyl ring help to extend the π-conjugation or does it break it?

Furthermore, we have focused our attention on oFL because they complement our previous studies on exTTF-oFL-C$_{60}$ conjugates[26] and allow us to assess the influence of another structural modification in oFL conjugates, namely, changing the electron donor. Together with the results on H$_2$P-oPPE-C$_{60}$/ZnP-oPPE-C$_{60}$ conjugates,[25] we now gain thorough insights into the electron-donating properties of porphyrins as incorporated into different

TABLE 1. Redox Potential Values Determined by Cyclic Voltammetry of 1a, 1b, 3a, 3b, 4a, 4b, and Reference Compounds[a]

compound	E_{red}^1	E_{red}^2	$E_{1/2,red}^3$	E_{red}^4	$E_{1/2,red}^5$	E_{ox}^1	E_{ox}^2	E_{ox}^3	E_{ox}^4	E_{ox}^5
Fl_2-CHO (**I**)	−2029[b]					1295	1608	1873		
Fl_3-CHO (**J**)	−2080					1114	1332	1800		
$(R)_4$-ZnP (**2**)	−1691[b]	−2045[b]				503 (455)[b,c]	884 (840)[b,c]			
$(R)_3$-ZnP-Fl_2 (**K**)	−1684[b]	−2042[b]				518 (459)[b,c]	903 (847)[b,c]	1282 (1217)[b,c]	1563	1803
$(R)_3$-ZnP-Fl_2-CHO (**1a**)	−1698[b]	−2158				519 (454)[b,c]	908 (837)[b,c]	1394 (1323)[b,c]	1726	
$(R)_3$-ZnP-Fl_3-CHO (**1b**)	−1693[b]	−2110				515 (454)[b,c]	933 (837)[b,c]	1145 (1098)[b,c]	1401	
C_{60}	−795[b]	−1191[b]	−1649	−2122[b]						
L	−912[b]	−1310[b]	−1849			1094	1545			
Fl_2-C_{60} (**M**)	−882[b]	−1293[b]	−1843	−2333		1170	1345	1623		
Fl_3-C_{60} (**N**)	−880[b]	−1292[b]	−1839			1096	1394	1809		
$(R)_3$-ZnP-Ph-Fl-C_{60} (**3a**)	−911[b]	−1325[b]	−1675	−1877[b]	−2026	543 (480)[b,c]	914 (851)[b,c]	1212	1480	1670
$(R)_3$-ZnP-Ph-Fl_2-C_{60} (**3b**)	−917[b]	−1333[b]	−1674	−1881[b]	−2026	528 (477)[b,c]	915 (852)[b,c]	1131	1286	1597
$(R)_3$-ZnP-Fl_2-C_{60} (**4a**)	−922[b]	−1336[b]	−1695	−1884[b]	−2042	503 (461)[b,c]	885 (843)[b,c]	1160	1492	1759
$(R)_3$-ZnP-Fl_3-C_{60} (**4b**)	−921[b]	−1338[b]	−1696	−1893[b]	−2065	520 (463)[b,c]	899 (843)[b,c]	1198	1557	

[a]Potentials in mV; scan rate 100 mV s^{-1}; glassy carbon working electrode, $Ag/AgNO_3$ reference electrode, Pt counter electrode; 0.1 M Bu_4NClO_4 in *o*DCB/CH_3CN (4:1 v/v). [b]Half wave potential values ($E_{1/2}$). [c]$E_{1/2}$ observed in partial scans.

multicomponent electron donor−acceptor conjugates. Additionally, if one considers the properties of previously published ZnP-oligo-thienylenevinylene (oTV)-C_{60},[36] H_2P-oPPE-C_{60}, and ZnP-oPPE-C_{60} conjugates,[37] the present study provides a comprehensive picture of (i) ZnP as electron donors and (ii) the molecular wire properties of oPPVs, oPPEs, oFLs, and oTVs in combination with porphyrins and fullerenes.

RESULTS AND DISCUSSION

Synthesis. The synthetic route toward **1a**, **1b**, **4a**, and **4b** is shown in Scheme 1. The classical method[38] of tetramerizing pyrrole and aldehydes (in this case 4-*tert*-butylbenzaldehyde and 7-bromo-9,9-dihexyl-9*H*-fluorene-2-carbaldehyde) was used to prepare **A**. Suzuki−Miyaura reaction of **A** with **B** and **C**,[39] respectively, gave the bifluorenyl and trifluorenyl derivatives **D** and **E** in 64 and 45% yields. Compounds **D** and **E** were converted into their zinc complexes **1a** and **1b**. Cycloadditions to C_{60} of the azomethine ylides,[40,41] formed *in situ* by reaction of the formyl group of **1a** and **1b** with sarcosine in refluxing chlorobenzene, led to the target fulleropyrrolidines **4a** and **4b** in 70−73% yields. Analogous synthetic protocols starting from porphyrin derivative **F** afforded the products **3a** and **3b** with an additional phenyl spacer group between the porphyrin and fluorene unit(s) (Scheme 2). Experimental details of the synthetic routes are provided in the Supporting Information.

Solution Electrochemical Studies. The electrochemical properties of **1a**, **1b**, **3a**, **3b**, **4a**, and **4b** were probed by room temperature cyclic voltammetric measurements in *o*-dichlorobenzene/acetonitrile solvent mixture. The redox potentials are collated in Table 1 together with those of pristine C_{60} and the reference compounds **I**, **J**, **K**, **L**, **M**, and **N** shown in Chart 1. Complexes **3a**,**b** and **4a**,**b** generate stable cation radicals and anion radicals when the scan was repeated in the region between −2300 and 1100 mV (Figure 2). First, five consecutive one-electron reduction waves—all *quasi*-reversible—have been observed during the reduction scan. A good correlation with reference compounds **M**, **N**, and *N*-methylfulleropyrrolidine **L** allows us to assign the first, second, and fourth reduction waves to C_{60}.[42,43] The third and fifth reduction waves can be assigned to the reduction of the ZnP core, due to correspondence with reference compounds **2** and **K**. The similarity of the reduction potentials with all of the reference compounds confirms the lack of substantial electronic interactions in the ground state. As expected,[44] shifts of the C_{60} reduction waves to more negative values, relative to pristine C_{60}, are observed

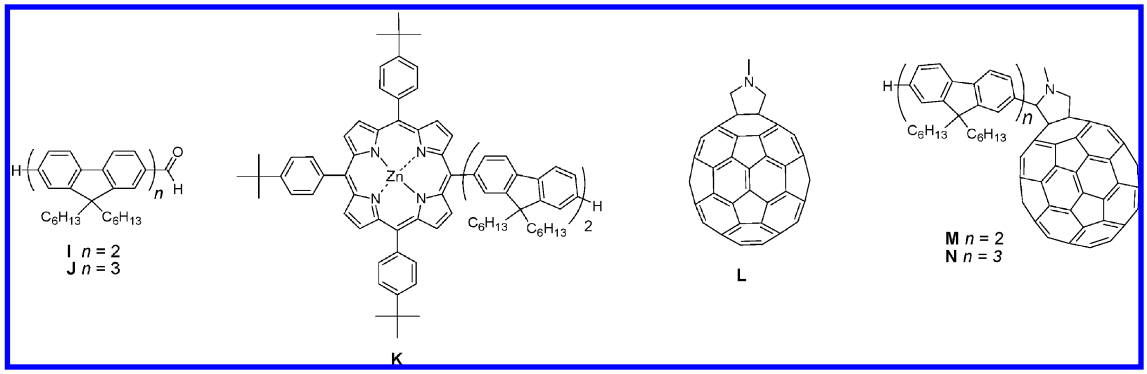

Chart 1. Reference compounds for electrochemical studies.

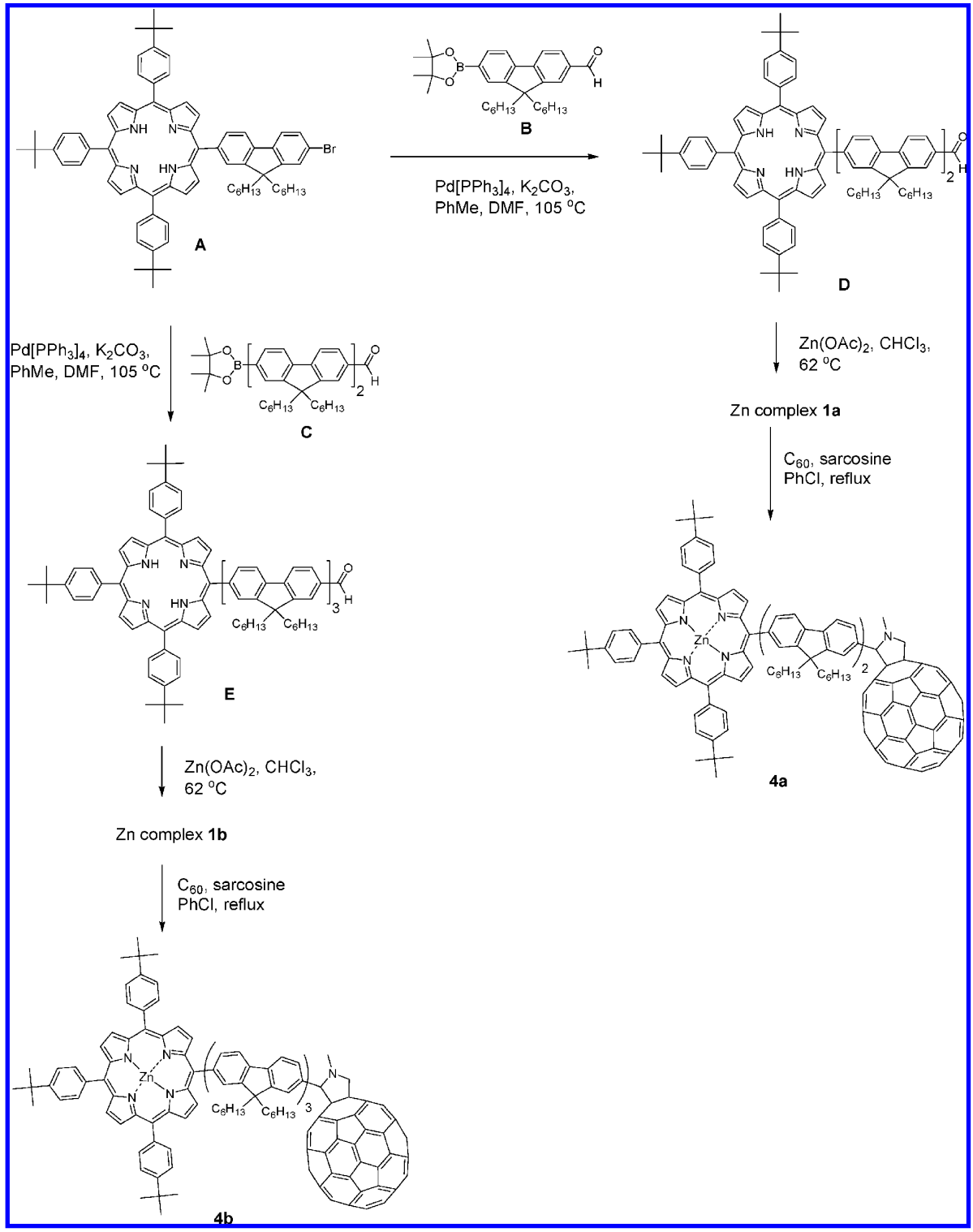

Scheme 1. Synthesis of 1a, 1b, 4a, and 4b.

for **3a**,**b** and **4a**,**b**. This is due to the saturation of a double bond on the fullerene core and the raised LUMO energy in **3a**,**b** and **4a**,**b**.

The second reduction wave of **1a**,**b** is irreversible, while the second waves of all other compounds containing ZnP are quasi-reversible. For **1a**,**b**, the reduction of the aldehyde group overlaps with the second reduction wave of the porphyrin moiety. On the reverse scan in the region of −2300 to 0 mV, three instead of two one-electron oxidation waves are observed. The oxidation waves of the aldehyde functionality and the porphyrin moiety are smaller (less current) than the overlapping reduction waves and are observed separately at E_{ox} −1870 and −1982 mV for **1a** and at E_{ox} −1845 and −1988 mV for **1b**. Therefore, the second reduction waves of **1a**,**b** are observed as an irreversible two-electron process. The quasi-

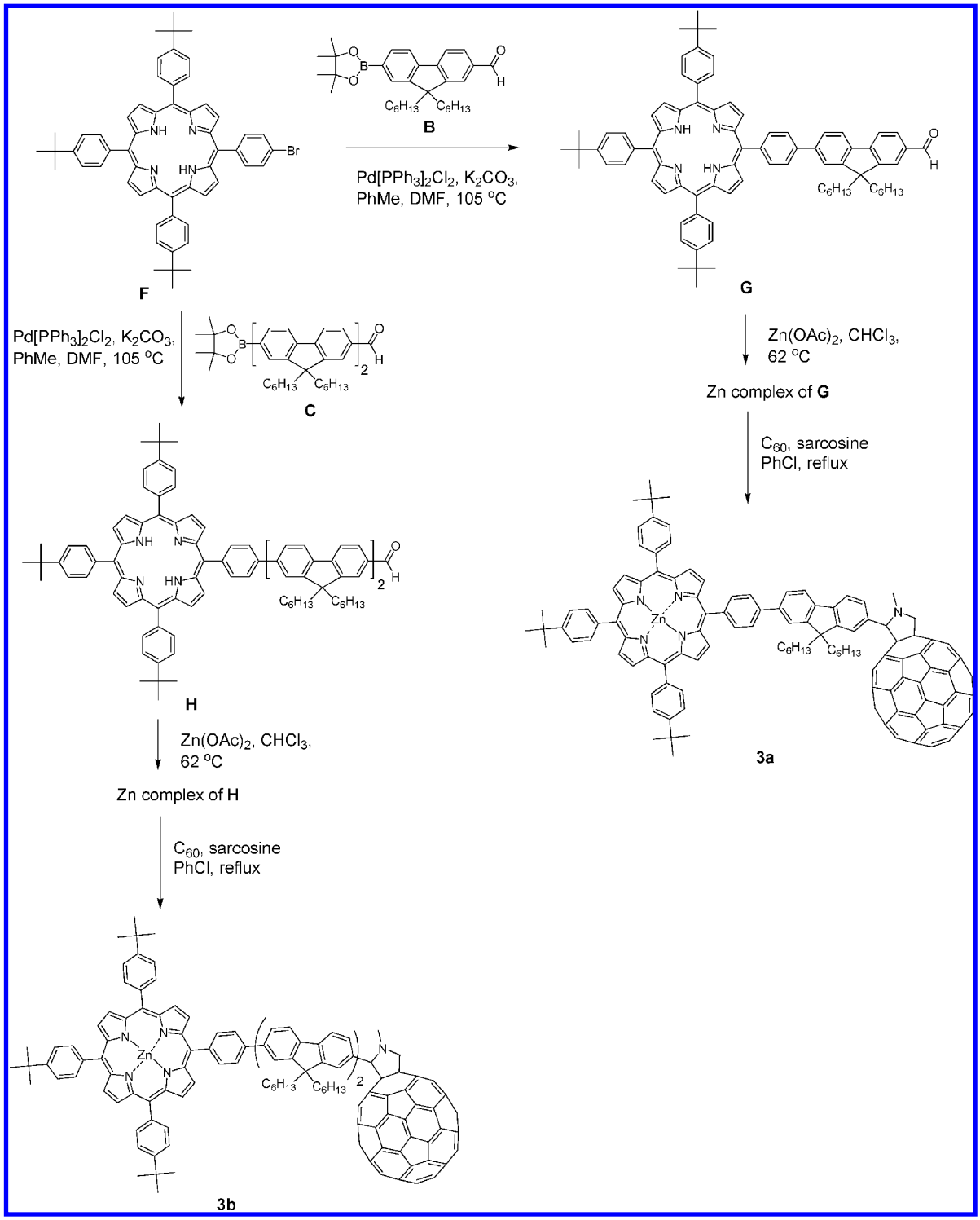

Scheme 2. Synthesis of 3a and 3b.

reversibility of **3a**,**b** and **4a**,**b** was investigated by performing three consecutive scans of each of the reduction waves. The CVs for **4b** are shown in Figure S4 in the Supporting Information.

On the oxidation scans, several quasi-reversible or irreversible oxidation waves were observed during the oxidation of **3a**,**b**, **4a**,**b**, and the relevant reference compounds when scanning beyond *ca.* 1 V. Scanning in the region of 0−1 V clearly indicates the quasi-reversibility of the first two waves observed in the compounds containing a ZnP unit (Figure 3). These initial oxidation waves of **3a**,**b** and **4a**,**b** can be assigned to the porphyrin moiety because of good agreement with reference compounds **2**, **K**, and **1a**,**b**. Similar to the reduction of the porphyrin moiety, no shifts in the oxidation potential were observed for the first two waves. The cation radical and dication formation are unaffected by the covalent link to oFL. The additional phenyl

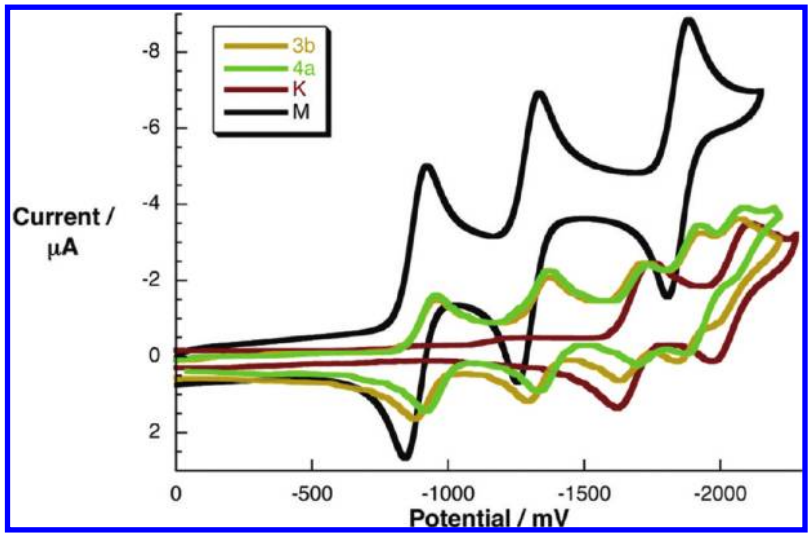

Figure 2. Reductive CVs of bifluorene derivatives 3b, 4a, K, and M (for conditions, see Table 1).

unit in **3a**,**b** leaves the strongest electron-donating moiety unaffected.

Molecular Modeling. The geometries of **3a**,**b** and **4a**,**b** (with methyl groups replacing hexyl) were optimized using the AM1[45] semiempirical Hamiltonian (see Supporting Information for details on the geometrical analysis and rotational barriers).

It was found that the conformations of all systems represent a structural compromise, which, on one hand, minimizes steric hindrance and, on the other, maximizes the π-conjugation pathway. As a consequence, the electronic communication between the donor and acceptor moieties is diminished and, thus, smaller charge recombination rates are expected.

Further insight into the charge-transfer properties of **3a**,**b** and **4a**,**b** is provided by analysis of the frontier orbitals. In particular, the highest occupied orbitals (HOMOs) and the lowest unoccupied orbitals (LUMOs) perfectly reflect the donor−acceptor character of ZnP and C_{60}. Density functional theory (DFT) calculations revealed important differences between the different oligomers. In the monomer **3a**, for instance, the HOMO is strongly localized on the ZnP donor moiety, whereas the HOMO of **4b** exhibits significant overlap of the electron density into the oFL bridge (Figure 4). This results in strong electronic coupling between the donor and the bridge in **4b** and, therefore, more facile electron injection from ZnP into the bridge. Thus, the bridge becomes more and more involved in the electron-transfer process with increasing oFL length, rather than being a passive spacer that just mediates the electronic coupling between donor and acceptor.[20]

Reference calculations on the oFL units themselves (*i.e.*, oFL_1, oFL_2, and oFL_3) strengthen these conclusions. The HOMO−LUMO gap in oFL_1 is 1.10 eV lower than in the corresponding oFL_3. This is simply because the LUMO energies of oFL become lower with increasing π-conjugation length. We may then postulate that, in line with the photophysical outcome, the charge-transfer mechanism may change with increasing donor−acceptor separation distance from superexchange tunneling to incoherent charge hopping. The orbital schemes of **3a** and **4b** are consistent with this hypothesis. Moreover, the energies of the lower-lying HOMO-1 and the HOMO orbitals strongly depend on oFL length (Figure 5). The HOMO-1 orbital in **3a** and **4a**, for instance, overlaps strongly with the oFL bridge moiety, whereas the HOMO is strongly localized on ZnP. On going from **3a** to **4b**, the separation between the HOMO-1 and HOMO orbital energies progressively vanishes with increasing oFL length. Finally, in **3b**, a switch between the electronic distributions of HOMO and HOMO-1 occurs. From this point on, the HOMO-1 orbital remains strongly localized on the ZnP donor and the HOMO orbital involves significant overlap with the linker. Hence, we may suggest that the superexchange mechanism will dominate the charge-transfer process in **3a** and **4a**, whereas in **3b** and **4b**, charge hopping is probably the mechanism of choice. As expected, the LUMOs in all systems are strongly localized on the C_{60} moiety, corroborating the function of C_{60} as electron acceptors. In addition, the LUMO energies of all ZnP-oFL-C_{60} conjugates match the LUMO energy of the C_{60} reference.

Semiempirical (AM1) configuration interaction (CI) calculations including single and double excitations (CISD) with an active window of five occupied and five unoccupied orbitals were performed to elucidate excited-state properties. The computations predict the HOMO to LUMO transition to be the major contribution to the charge-transfer processes with a donor−acceptor distance-dependent

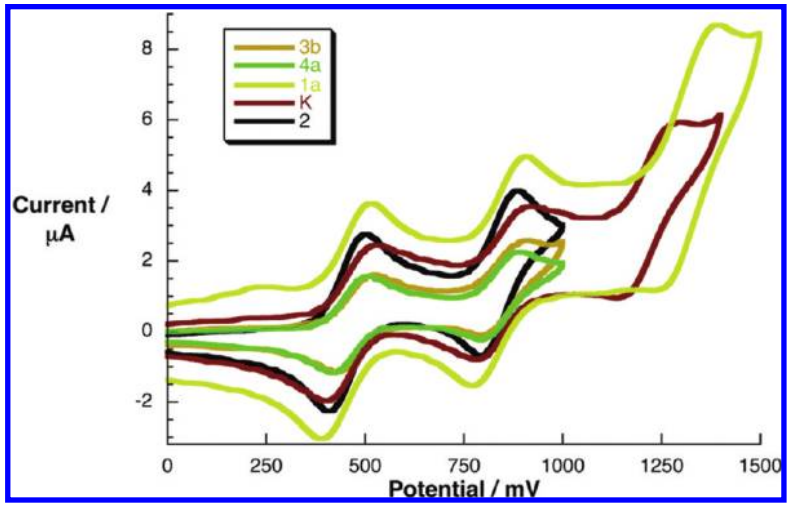

Figure 3. Oxidative CVs of compounds 1a, 2, 3b, 4a, and K. For conditions, see Table 1.

Figure 4. HOMO (left) and LUMO (right) orbitals of 3a (top) and 4b (bottom) resulting from DFT calculations.

change of dipole moment: 71.7 D for **3a**; 121.7 D for **4a**; 160.8 D for **3b**; 198.7 D for **4b** (Table S1, Supporting Information). Visualizing the molecular electrostatic potential of the charge-separated states confirms that ZnP is the electron-donating moiety and C_{60} is the acceptor. In all conjugates, the positive charge was found to be localized on ZnP and the negative one on C_{60} (Figure 6, top). In addition, we obtained charge-transfer (CT) states, in which the positive charge is localized on oFL (Figure 6, bottom). The excitation energies of these bridge charge-transfer (BCT) states are well-separated from the excitation energies of the major HOMO−LUMO transitions in **3a** and **4a**. However, in **3b** and **4b**, the excitation energies of the BCT states approach those of the major CT states. From these findings, we deduce that with increasing temperature a thermally induced mixing of the linker eigenstates and the donor eigenstates can set in. As a consequence, excitations of the linker may contribute to the overall charge-transfer processes. Moreover, lengthening the oFL linker will have an equivalent effect on the charge transfer. In other words, the mixing of the BCTs and CTs becomes progressively allowed in energy with increasing length of the π-conjugated pathway. Lower bridge LUMOs and a longer π-conjugation pathway resulting from a larger number of repeat units of the linker favor incoherent charge hopping at higher temperatures. In **3a**, the major CT transition arises from HOMO → LUMO and HOMO-1 → LUMO excitations. This is because strong frontier orbital interactions dominate at short

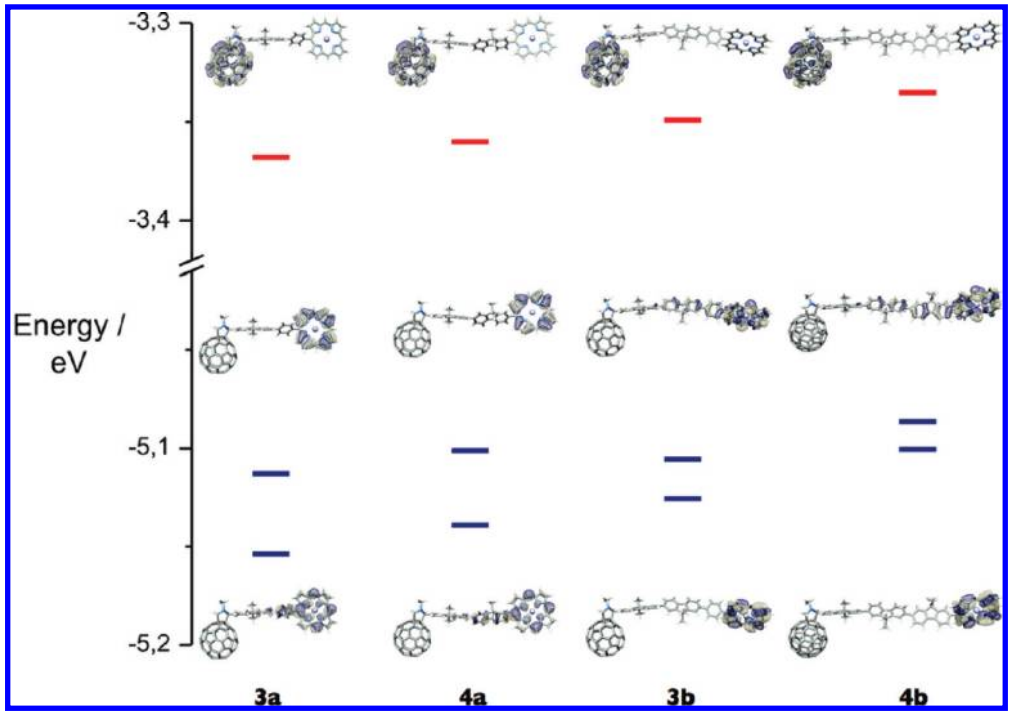

Figure 5. B3LYP/6-31G(d,p) energies of lower-lying HOMO (blue) and LUMO (red) orbitals of the different triads with the corresponding representations of the HOMO and HOMO-1 resulting from DFT calculations.

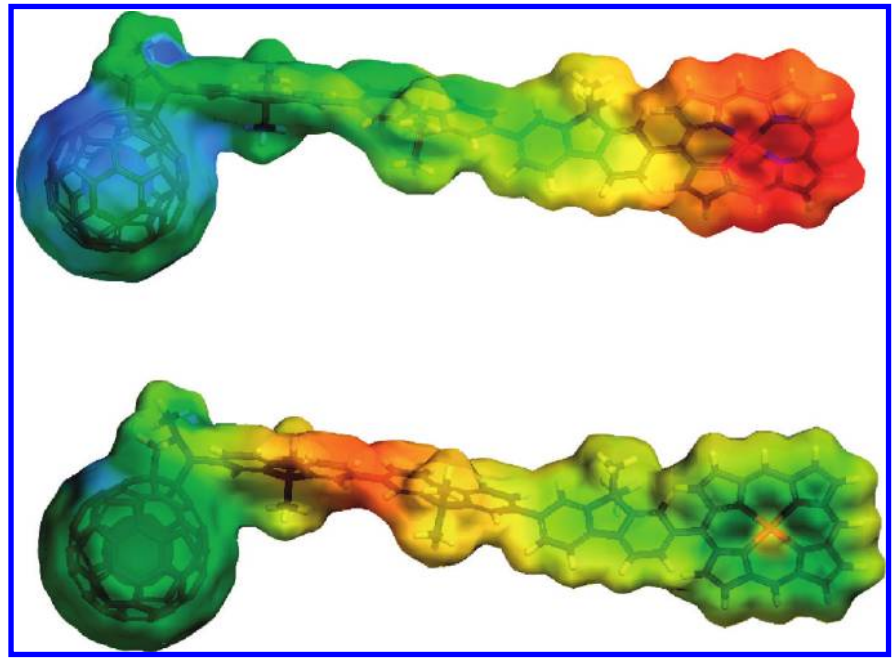

Figure 6. Representative visualization of the electrostatic potentials of the first charge-transfer state (CS, top) and the bridge charge-transfer state (BCT, bottom) of 4b.

donor−acceptor distances. Hence, a charge transfer *via* the superexchange mechanism is favored.

In short, our calculations suggest that the charge-transfer mechanism changes as a function of temperature and chemical structure of the linker. Switching between coherent superexchange tunneling and incoherent charge hopping is expected to occur when the temperature is increased or the length of the π-conjugated electron-transfer pathway changes.

Photophysics. To shed light on the electronic interactions between the photo- and redox-active components (*i.e.*, ZnP, oFL, and C_{60}), the ground-state absorption spectra of the different ZnP-oFL-C_{60} conjugates were compared with those of the individual components. In essence, the absorption spectra of the conjugates are best described as simple superimpositions of the component spectra, lacking significant perturbations or additional charge-transfer transitions. A detailed description of the absorption features is found in the Supporting Information. Important in this context is that the insertion of additional phenyl rings between ZnP and oFL in **3a**,**b** alters the π-system of the different ZnP-oFL-C_{60} conjugates without, however, interrupting the conjugation between the donor and the linker. Support for this notion is derived from the linear dependence of the red-shifted absorption maxima on the length of the linker (Figure S3).

To study the electronic interactions between the photo- and redox-active components (*i.e.*, ZnP, oFL, and C_{60}) in the excited state, emission measurements were carried out in solvents of different polarity (*i.e.*, toluene, THF, and benzonitrile). The data are always set in relation to the individual building blocks.

The weakest chromophore among the photoactive constituents is C_{60} (1.76 eV). Excitation of it, for example, at 355 nm generates a rather broad emission in the 650 to 850 nm range. The short wavelength maximum at 710 nm is an excellent match of the long wavelength absorption maximum at 695 nm. Noteworthy are the low quantum yields of the C_{60} fluorescence with values of around 6×10^{-4}, inferring that the major deactivation pathway is, in fact, intersystem crossing (*vide supra*).[46] From complementary fluorescence lifetime measurements, we derived a lifetime of 1.4 ns, by which the singlet excited state of C_{60} decays directly to the singlet ground state. With a quantum yield of 0.04, ZnP is an appreciably stronger fluorophore (2.1 eV). A typical fluorescence spectrum includes peaks at 600 and 650 nm. Following the fluorescence at both of these maxima as a function of time enabled a determination of the ZnP fluorescence lifetime as 2.3 ns in several solvents. Far more intense emissions were recorded for oFL (2.82 eV). In light of the strong ground-state absorption, 345 nm was chosen for photoexcitation. The broad fluorescence maximizes around 460 nm and has a quantum yield of 0.68.

As Figure 7 demonstrates, the ZnP fluorescence dominates the spectral range between 550 and 750 nm in **1a**,**b**. In particular, linking oFL to ZnP has a substantial impact on the fluorescence quantum yields of the former (8.3×10^{-4}), while it exerts almost no appreciable impact on the fluorescence quantum yields of the latter (0.04).[37] This implies an oFL excited-state deactivation *via* photosensitization of ZnP. Evidence that this energy transfer indeed takes place comes from a set of excitation measurements. The excitation spectrum of the ZnP fluorescence in **1a**,**b** is virtually identical with

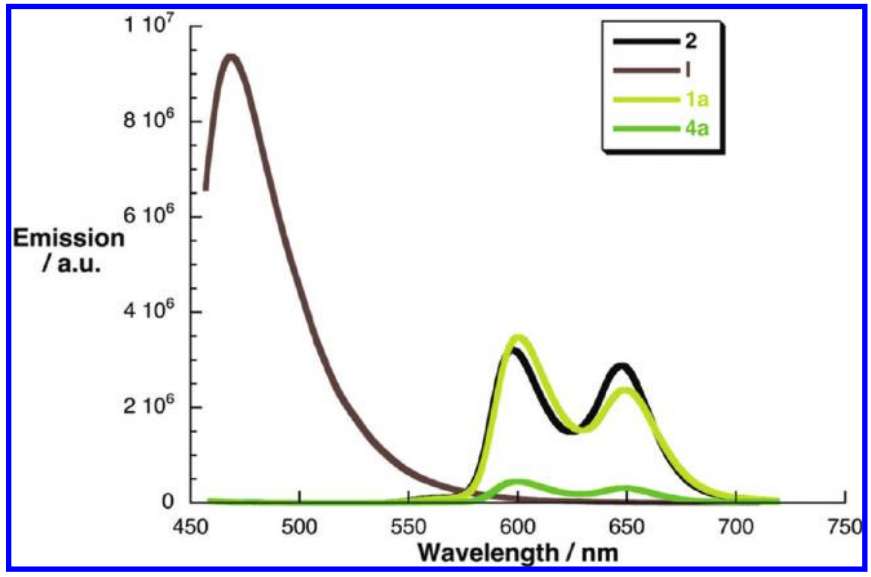

Figure 7. Room temperature fluorescence spectra of 2, I, 1a, and 4a in toluene upon 345 nm excitation.

the ground-state absorption and the excitation spectra of the reference compounds **I**, **J**, and **2**.

In sharp contrast, attaching C_{60} causes a dramatic decrease in the ZnP fluorescence intensity of **3a**,**b** and **4a**,**b** (Figure 7)—independent of the excitation wavelengths, that is, 345 nm for oFL and 420 nm for ZnP. In toluene, the quantum yield is only 1.0×10^{-3} upon 345 nm excitation. Important is that, although the yield drops, the emission patterns of ZnP are not affected by the presence of the electron-accepting C_{60}. Implicit is a strongly exothermic charge-transfer deactivation, during which the ZnP singlet excited state is readily transformed into a radical ion pair with high energy (1.82 eV). A closer inspection reveals that the quenching strongly depends on the length of the oFL linker. Strongest quenching with a quantum yield of 8.0×10^{-4} in toluene was found in **3a**. Compound **4b**, on the other hand, with a quantum yield in toluene of 2.0×10^{-2} quenches the reference fluorescence only by a factor of 2. Contrasting 420 nm excitation (*i.e.*, ZnP) with 345 nm excitation (*i.e.*, oFL) leads to a 10-fold difference in quantum yields, 10^{-2} *versus* 10^{-3}. However, instead of correlating these values with different deactivation dynamics of the ZnP singlet excited state (*i.e.*, the singlet excited-state lifetimes would depend on the excitation wavelength), it is more likely that the ZnP singlet is formed in different yields. In fact, the presence of C_{60} leads to a competitive deactivation scenario, that is, energy transfer to ZnP *versus* energy transfer to C_{60}.

Upon modifying the solvent polarity from toluene ($\varepsilon = 2.38$) *via* THF ($\varepsilon = 7.6$) to benzonitrile ($\varepsilon = 24.8$), a gradual intensification of the ZnP fluorescence quenching is discernible for **3a**,**b** and **4a**,**b**. In THF, the quantum yields are, for example, 2.4×10^{-4} for **3a** and 1.2×10^{-2} for **4b**. In particular, a better solvation of charged species in the more polar media results in (i) lower energies of the radical ion pair states and (ii) larger energy gaps relative to the excited singlet state. Thus, the trend in solvent polarity is attributed to intramolecular charge-transfer interactions, which are facilitated by larger driving forces.

Relating the fluorescence quantum yields in the donor−acceptor ensemble, Φ_{dyad}, to that of ZnP, $\Phi_{reference}$, and their lifetime, $\tau_{reference}$, helps to determine the rate constants for fluorescence deactivation:[47]

$$k = [\Phi_{reference} - \Phi_{dyad}]/[\tau_{reference}\Phi_{dyad}] \qquad (1)$$

The rate constants are listed in Table 2. Noteworthy, the fast charge-transfer rates (*i.e.*, up to 10^{-9} s^{-1}), as they were determined *via* this relation, infer a reasonable electronic coupling between ZnP as electron donor and C_{60} as electron acceptor.

An independent probe for the magnitude of charge-transfer quenching is fluorescence lifetime experiments. For this, we recorded the 600 nm maximum of the fluorescence in ZnP. Importantly, fluorescence lifetime experiments allow the contributions of ZnP to be segregated from those of oFL and C_{60}. In general, the fluorescence decay curves of ZnP were best fitted by a single exponential decay law. For ZnP, the lifetimes were 2.14 ns (toluene), 2.2 ns (THF), and 2.08 ns (benzonitrile). As Table 2 indicates, for most ZnP-oFL-C_{60} conjugates, the fluorescence lifetimes fall between 0.69 and 2.06 ns in THF. Important is the solvent depen-

TABLE 2. Singlet Excited-State Lifetimes (τ_S), Fluorescence Lifetimes (τ_F), Charge Separation (k_{cs}), and Charge Recombination (k_{cr}) Rates

	τ_S [ns]	τ_F [ns]		k_{cs} [s^{-1}]		k_{cr} [s^{-1}]	
	THF	THF	PhCN	THF	PhCN	THF	PhCN
3a	0.96	0.69	0.25	1.5×10^9	3.6×10^9	2.2×10^6	2.9×10^6
4a	1.08	1.25	0.65	7.7×10^8	1.1×10^9	1.5×10^6	2.3×10^6
3b	1.21	1.52	0.94	6.0×10^8	6.5×10^8	1.1×10^6	1.3×10^6
4b	1.60	2.06	1.27	4.5×10^8	3.7×10^8	5.0×10^5	6.1×10^5

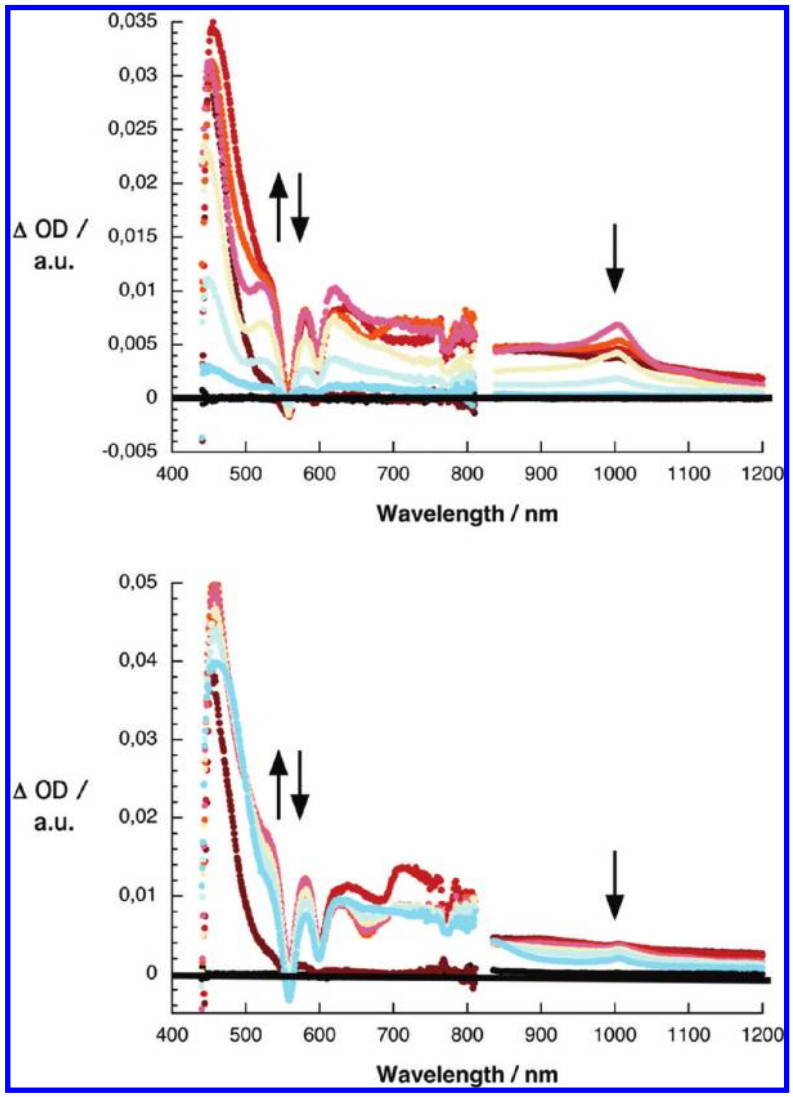

Figure 8. Differential absorption spectra (visible and near-infrared) obtained upon femtosecond flash photolysis (420 nm to 150 nJ) of 3a (top) and 4b (bottom) in argon-saturated THF with several identical time delays between 0 and 3000 ps at room temperature. These spectra illustrate the instantaneous formation of the π-radical cation of ZnP ($ZnP^{\bullet+}$, 480−700 nm) and the one-electron reduced anion of C_{60} ($C_{60}^{\bullet-}$, 1010 nm).

dence, leading to an acceleration of the fluorescence deactivation. Taking the aforementioned in context, it suggests indeed a rapid charge-transfer deactivation of the photoexcited ZnP with rates that are between 10^8 and 10^9 s^{-1}.

Transient absorption measurements were deemed necessary to confirm the photoproducts of **3a**,**b** and **4a,b**. Due to overlapping absorptions of ZnP, oFL, and C_{60}, we have focused first on the selective excitation of ZnP.

In **1a**,**b**, despite the unequivocal excitation of oFL, no spectral evidence for the oFL singlet−singlet absorption around 725 nm was found after the laser excitation. Instead, the spectral features are identical with the spectral fingerprints of the ZnP singlet excited state.[48,49] Specifically, characteristic maxima at 460, 580, and 630 nm, as well as minima at 565 and 605 nm, are clear attributes of the ZnP singlet−singlet absorption. The rise time of, for example, the 630 nm absorption, representing the actual energy-transfer event, is, however, masked by the instrument response time and, therefore, prevents a meaningful kinetic analysis of the intramolecular reaction. On a longer time scale (0−3 ns), the fate of the ZnP singlet excited state is identical to that, which has already been described, namely, intersystem crossing, driven by a strong spin−orbit coupling, governs the transformation (10^8 s^{-1}) of the singlet into the triplet excited state. The latter was identified by a long-lived and strongly absorbing triplet−triplet transition at 840 nm.

Regarding the femtosecond transient absorption measurements of **3a**,**b** and **4a**,**b**, immediately after the laser excitation, the strong singlet−singlet absorptions of ZnP start to emerge with about 1×10^{12} s^{-1}. This confirms the successful formation of the ZnP singlet excited states. However, instead of seeing the slow intersystem crossing (ISC) process, the singlet−singlet absorptions decay in the presence of the electron-accepting C_{60} with accelerated dynamics. The singlet excited-state lifetimes, as they were determined from an average of first-order fits of the time absorption profiles at various wavelengths, are listed in Table 2, and some representative examples are given in Figures 8 and 9. An important aspect is that the singlet excited-state lifetimes match quantitatively those values derived in the fluorescence experiments—both steady-state and time-resolved.

Spectroscopically, the transient absorption changes, taken after the completion of the decay, bear no resemblance with any triplet excited state (*i.e.*, ZnP, oFL, and C_{60}). In particular, in THF, the broad absorption in the 600−700 nm region corresponds to the one-electron oxidized $ZnP^{\bullet+}$,[50] while in the near-infrared region, the 1000 nm maximum resembles the signature of the one-electron reduced $C_{60}^{\bullet-}$.[46] The acceleration of the charge transfer upon increasing the solvent polarity should also be mentioned (see Table 2), a finding that suggests charge-transfer dynamics in the normal region of the Marcus parabola.[51]

The $ZnP^{\bullet+}$-oFL-$C_{60}^{\bullet-}$ radical ion pair states are persistent on the picosecond time scale and start to decay only in the nanosecond time regime. The charge recombination rates were easily determined from complementary nanosecond experiments upon excitation with a 6 ns laser pulse. The spectral signatures of the one-electron oxidized $ZnP^{\bullet+}$ radical cation and the one-electron reduced $C_{60}^{\bullet-}$ radical anion, as detected imme-

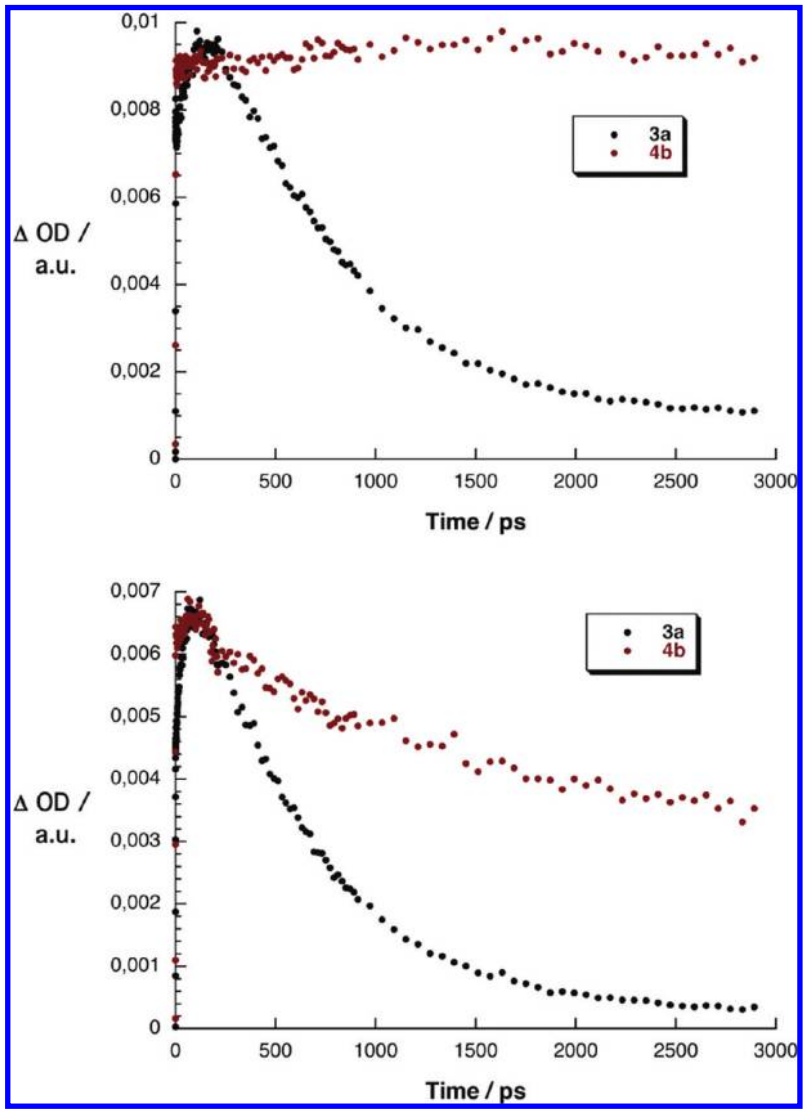

Figure 9. Time profiles at 630 nm (top) and 1010 nm (bottom) of the differential absorption spectra of 3a (black) and 4b (red) reflecting the dependence of the charge separation dynamics on the length of the oFL linker.

diately after the laser pulse, decay synchronously and give rise to kinetics that obey a clean unimolecular rate law. Lifetimes of 445 and 654 ns were obtained in THF for **3a** and **4a**, respectively, where the electron transfer is assumed to follow the superexchange tunneling mechanism. Our molecular modeling suggests that with increasing bridge length (**3b** *versus* **4b**) the HOMO orbital involves significant overlap with oFL and BCT states of lower energy. Hence, incoherent charge hopping leads to longer lifetimes of 952 and 1990 ns for **3b** and **4b**, respectively. In close agreement with this hypothesis is the temperature dependence (*vide supra*).

The analysis of the charge-transfer rates (*i.e.*, charge separation and charge recombination) enabled a determination of the β factors for the different ZnP-oFL-C_{60} conjugates. Plotting the rates as a function of donor−acceptor distance, R_{DA} results in linear relationships from which $\beta = 0.097$ Å^{-1} emerged, a value in close agreement with a recent investigation of oFL that is linked to C_{60} and electron-donating exTTF.[13] Of particular importance is that the same β values were obtained for the charge separation and charge recombination processes in THF as well as in benzonitrile. Consequently, the charge-transfer features may be attributed to the intrinsic properties of the bridge.

To shed light on the deactivation mechanisms in **3a**,**b** and **4a**,**b**, we have probed the temperature dependence of the fluorescence quenching in the range between 273 and 353 K. At first glance, the measurements revealed that the ZnP fluorescence quantum yields increase gradually with increasing temperature. A closer analysis establishes that the quantum yields are also impacted by the length of the oFL linker. In general, at low temperatures (*i.e.*, 273−298 K), weak dependence of the quantum yields on temperature is observed for all conjugates. Above room temperature (*i.e.*, 298−353 K), the situation changes and depends on the oFL length. At longer donor−acceptor separation distances, namely, in **3b** and **4b**, the quantum yields vary significantly with temperature. On the contrary, short donor−acceptor separations, as present in **3a**, lead to very minor temperature dependences. A likely rationale for this observation involves the oFL LUMOs as the HOMO−LUMO gap is reduced upon increasing the linker length. As a direct consequence, the linker LUMOs may be accessed from the ZnP HOMOs due to comparable orbital energies. Likewise, an increase in temperature lowers the oFL LUMOs. Accordingly, in **3b** and **4b**, the incoherent hopping mechanism is the most probable operative mode for the charge-transfer process, thus changing the temperature strongly impacts the rate of charge transfer. In **3a** and **4a**, on the other hand, the shorter donor−acceptor distance leads to a superexchange mechanism with charge separation rates that are almost independent of temperature (Figure 10). In sound agreement with the theoretical studies, which propose a mixing of BCT states of lower energies with the CT states in **3b** and **4b**, we may assume that increasing the temperature helps

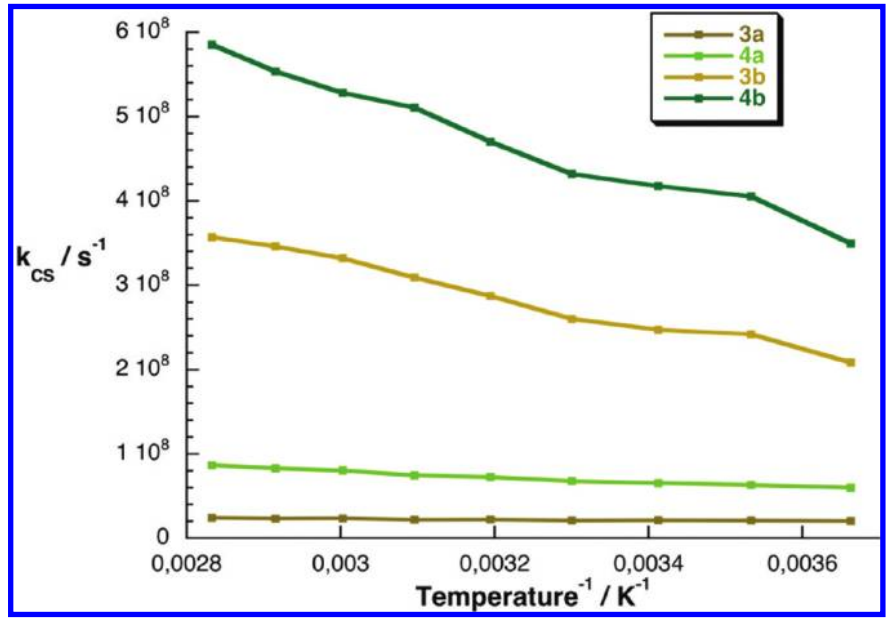

Figure 10. Temperature dependence of the charge separation for 3a,b and 4a,b in the 273 to 353 K temperature regime based on the temperature-dependent fluorescence experiments in benzonitrile.

to overcome the thermodynamic barrier to form C_{60}-oFL$^{\bullet-}$-ZnP$^{\bullet+}$. Molecular modeling suggests that this barrier is much easier to overcome at large donor−acceptor separation distances due to the increasing π-conjugation and lower charge injection energies. Hence, the strong temperature dependence observed for **3b** and **4b** suggests a thermally activated charge hopping.

Clearly, the temperature dependence infers an appreciable acceleration of the charge separation dynamics for the longer bridged C_{60}-oFL-ZnP. In sound agreement with the theoretical studies, which imply mixing of BCT of lower energy states with CT states in **3b** and **4b**, increasing the temperature facilitates overcoming the thermodynamic barriers to form C_{60}-oFL$^{\bullet-}$-ZnP$^{\bullet+}$. From the slopes of the corresponding Arrhenius plots ($\log(k_{CS}T^{1/2})$ *vs* T^{-1}), we have derived the following activation barriers: 0.055 eV for **3b**; 0.059 eV for **4b**. These values are slightly lower than the HOMO (ZnP)−HOMO (oFL) energy gap due to solvent stabilization.[52]

Moreover, the β values at different temperatures disclose an eminent increase with temperature with values that range from 0.097 Å^{-1} at 273 K to 0.160 Å^{-1} at 353 K. This agrees with the fact that at lower temperatures electron tunneling *via* superexchange is the operative mode with an overall weak distance dependence. Further support for this notion comes from the fact that the electronic levels of the bridge couple only weakly to the donor and acceptor and are separated by a reasonably high energy gap from the donor and acceptor frontier orbital levels. At higher temperatures, the linker eigenstates become accessible and we observe localized hopping due to strong vibronic coupling between donors, linkers, and acceptors. Here, a thermally activated charge hopping with stronger distance dependence sets in.

Plotting the charge-transfer rates *versus* the donor−acceptor distances of **3a**,**b** and **4a**,**b** provides an average picture of the systems, namely, with and without an additional phenyl ring (Figure 11). However, the phenyl rings of **3a** and **3b** are not simple extensions of the oFL bridge, but should instead be treated as separate building blocks inserted into ZnP-oFL-C_{60}. Consequently, two attenuation factors have to be considered: one for **3a**,**b** and one for **4a**,**b** (see Figure 11). In this regard, the slopes give rise to β values of 0.11 and 0.07 Å^{-1} in **3a**,**b** and **4a**,**b**, respectively. In **4a**,**b**, the oFL guarantees a homogeneous distribution of π-electrons and an extension of the conjugated orbitals into the electronic system of the donor. In other words, oFL provides an excellent π-electron pathway to transfer charges between donor and acceptor, affording a low attenuation factor. On the other hand, in **3a**,**b**, the additional phenyl ring perturbs the homogeneous oFL π-conjugation, creating a bottleneck for the electrons to pass. For that reason, charge separation is slower and charge recombination is faster, which is reflected in the increased values of β. Similar findings have already been revealed in the investigation of oPPE linking C_{60} and exTTF.[11] The high polarizability and the shorter bond lengths of the triple bonds in the oPPE wires prevent an extension of the homogeneous π-electron pathway from donor to acceptor, and no charge separation could be observed beyond 22 Å.

CONCLUSIONS

A series of new ZnP-wire-C_{60} conjugates, in which oFL bridges are covalently bound to electron-donating ZnP and electron-accepting C_{60}, have been synthesized

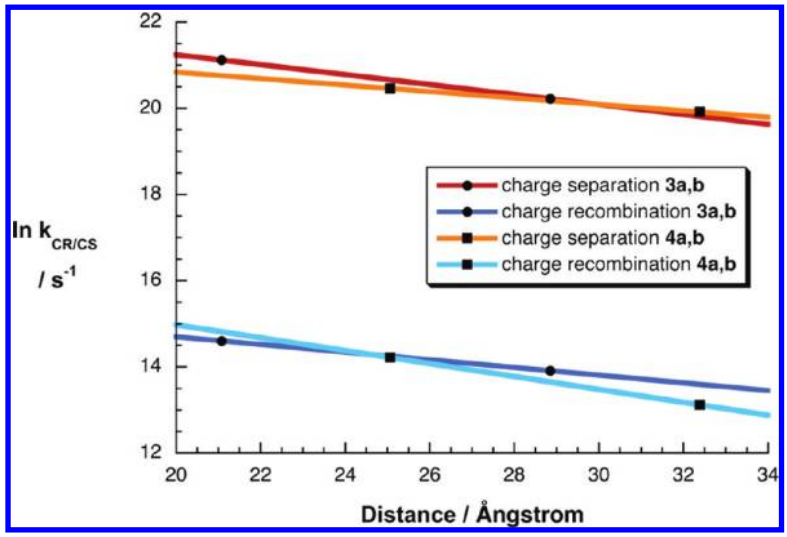

Figure 11. Dependence of center-to-center distances (R_{CC}) of the charge separation (ln k_{CS}) and charge recombination (ln k_{CR}) rate constants in nitrogen-saturated THF at room temperature, in relation to the structural differences between 3a,b and 4a,b. The slopes represent the different β values.

and characterized. Photoexcitation of either ZnP or oFL results in charge-transfer reactions over distances beyond 30 Å from the electron-donating ZnP to the electron-accepting C_{60} moiety in toluene, THF, and benzonitrile. Long-lived radical ion pair states with lifetimes in the microsecond time regime have been obtained. Furthermore, the lifetimes of the radical ion pairs depend on the length of the oFL linker. Most importantly, the quantum chemical and photophysical studies evidently propose that the rate of charge separation and also the operating charge-transfer mechanism are strongly dependent on the length of the linker between donor and acceptor as well as by the temperature and may be tuned by these variables. Calculations have shown that in systems with large donor−acceptor distances charge separation is expected to occur on the basis of incoherent charge hopping due to decreasing LUMO energies. On the other hand, decreasing the oFL length leads to superexchange tunneling due to closer donor−acceptor spacing. Further, at short donor−acceptor distances, the energies of the bridge charge-transfer (BCT) states are well-separated from the major HOMO → LUMO transitions. With increasing donor−acceptor distance, the excitation energies of the BCT states approach the excitation energies of the major charge-transfer states. Temperature-dependent photophysical experiments have shown that increasing the temperature facilitates the mixing of the BCTs and CTs and incoherent charge hopping becomes more and more probable. An analysis of the charge separation and charge recombination rate constants gives a temperature-dependent attenuation factor of $\beta = 0.097$ Å^{-1}.

Finally, the correlation of the attenuation factor β to the connection pattern between the ZnP donor and the oFL bridge revealed that linkers that consist of equal oFL building blocks provide a homogeneous distribution of the π-electrons and an extension of the conjugated orbitals onto the electronic system of the donor, which gives an excellent π-electron pathway for the electrons and low attenuation factors.

Acknowledgment. This work was supported by the Deutsche Forschungsgemeinschaft (SFB and Clusters of Excellence Engineering of Advanced Materials) and the EC FP7 ITN "FUNMOLS" Project No. 212942.

Supporting Information Available: Synthetic details and characterization of all compounds and reference compounds, details on theoretical methods, supplementary photophysical and theoretical characterization, and additional figures and tables. This material is available free of charge *via* the Internet at http://pubs.acs.org.

REFERENCES AND NOTES

1. Jortner, J., Ratner, M., Eds. *Molecular Electronics*; Blackwell: London, 1997.
2. Joachim, C.; Gimzewski, J. K.; Aviram, A. Electronics Using Hybrid-Molecular and Mono-molecular Devices. *Nature* **2000**, *408*, 541–548.
3. Troisi, A.; Ratner, M. A. Molecular Signatures in the Transport Properties of Molecular Wire Junctions: What Makes a Junction "Molecular"? *Small* **2006**, *2*, 172–181.
4. Scandola, F.; Chiorboli, C.; Indelli, M. T.; Rampi, M. A. In *Electron Transfer in Chemistry*; Balzani, V., Ed.; Wiley-VCH: Weinheim, Germany, 2001; Vol. III, Chapter 2.1.
5. De Cola, L.; Belser, P. In *Electron Transfer in Chemistry*; Balzani, V., Ed.; Wiley-VCH: Weinheim, Germany, 2001; Vol. V, Chapter 3.
6. Davis, W. B.; Svec, W. A.; Ratner, M. A.; Wasielewski, M. R. Molecular-Wire Behavior in *p*-Phenylenevinylene Oligomers. *Nature* **1998**, *396*, 60–63.
7. Wasielewski, M. R. Energy, Charge, and Spin Transport in Molecules and Self-Assembled Nanostructures Inspired by Photosynthesis. *J. Org. Chem.* **2006**, *71*, 5051–5066.
8. Aviram, A. Molecules for Memory, Logic, and Amplification. *J. Am. Chem. Soc.* **1988**, *110*, 5687–5692.
9. Carrol, L.; Gorman, C. B. The Genesis of Molecular Electronics. *Angew. Chem., Int. Ed.* **2002**, *41*, 4378–4400.
10. Review: Albinsson, B.; Eng, M. P.; Pettersson, K.; Winters, M. U. Electron and Energy Transfer in Donor−Acceptor Systems with Conjugated Molecular Bridges. *Phys. Chem. Chem. Phys.* **2007**, *9*, 5847–5864.
11. James, D. K.; Tour, J. M. Electrical Measurements in Molecular Electronics. *Chem. Mater.* **2004**, *16*, 4423–4435.
12. Creager, S.; *et al.* Electron Transfer at Electrodes through Conjugated "Molecular Wire" Bridges. *J. Am. Chem. Soc.* **1999**, *121*, 1059–1064.
13. Grozema, F. C.; Berlin, Y. A.; Siebbeles, L. D. A. Mechanism of Charge Migration through DNA: Molecular Wire Behavior, Single-Step Tunneling or Hopping. *J. Am. Chem. Soc.* **2000**, *122*, 10903–10909.
14. Jortner, J.; Bixon, M.; Langenbacher, T.; Michel-Beyerle, M. E. Charge Transfer and Transport in DNA. *Proc. Natl. Acad. Sci. U.S.A.* **1998**, *95*, 12759–12765.
15. Lambert, C.; Noll, G.; Schelter, J. Bridge-Mediated Hopping or Superexchange Electron-Transfer Processes in Bis(triarylamine) Systems. *Nat. Mater.* **2002**, *1*, 69–73.
16. Wasielewski, M. R.; Ratner, M. A.; Mujica, V.; Nitzan, A.

Electron Transfer Rates in Bridged Molecular Systems: A Phenomenological Approach to Relaxation. *J. Phys. Chem. A* **1997**, *101*, 6158–6164.
17. Gray, H. B.; Winkler, J. R. Long-Range Electron Transfer. *Proc. Natl. Acad. Sci. U.S.A.* **2005**, *102*, 3534–3539.
18. Albinsson, B.; Martensson, J. Long-Range Electron and Excitation Energy Transfer in Donor−Bridge−Acceptor Systems. *J. Photochem. Photobiol. C* **2008**, *9*, 138–155.
19. Weiss, E. A.; Wasielewski, M. R.; Ratner, M. A. Molecules as Wires: Molecule-Assisted Movement of Charge and Energy. *Top. Curr. Chem.* **2005**, *257*, 103–133.
20. Ratner, M. A. Bridge-Assisted Electron Transfer: Effective Electronic Coupling. *J. Phys. Chem.* **1990**, *94*, 4877–4883.
21. Giacalone, F.; Segura, J. L.; Martín, N.; Guldi, D. M. Exceptionally Small Attenuation Factors in Molecular Wires. *J. Am. Chem. Soc.* **2004**, *126*, 5340–5341.
22. Giacalone, F.; Segura, J. L.; Martín, N.; Ramey, J.; Guldi, D. M. Probing Molecular Wires: Synthesis, Structural, and Electronic Study of Donor−Acceptor Assemblies Exhibiting Long-Range Electron Transfer. *Chem.—Eur. J.* **2005**, *11*, 4819–4834.
23. Atienza, C.; Martín, N.; Wielopolski, M.; Haworth, N.; Clark, T.; Guldi, D. M. Tuning Electron Transfer through *p*-Phenyleneethynylene Molecular Wires. *Chem. Commun.* **2006**, *236*, 3202–3204.
24. Wielopolski, M.; Atienza, C.; Clark, T.; Guldi, D. M.; Martín, N. *p*-Phenyleneethynylene Molecular Wires: Influence of Structure on Photoinduced Electron-Transfer Properties. *Chem.—Eur. J.* **2008**, *14*, 6379–6390.
25. Lembo, A.; Tagliatesta, P.; Guldi, D. M.; Wielopolski, M.; Nuccetelli, M. Porphyrin-β-Oligo-ethynylenephenylene-[60]Fullerene Triads: Synthesis and Electrochemical and Photophysical Characterization of the New Porphyrin-Oligo-PPE-[60]Fullerene Systems. *J. Phys. Chem. A* **2009**, *113*, 1779–1793.
26. Atienza-Castellanos, C.; Wielopolski, M.; Guldi, D. M.; van der Pol, C.; Bryce, M. R.; Filippone, S.; Martín, N. Determination of the Attenuation Factor in Fluorene-Based Molecular Wires. *Chem. Commun.* **2007**, *48*, 5164–5166.
27. Goldsmith, R. H.; Sinks, L. E.; Kelley, R. F.; Betzen, L. E.; Liu, W. H.; Weiss, E. A.; Ratner, M. A.; Wasielewski, M. R. Wire-like Charge Transport at Near Constant Bridge Energy through Fluorene Oligomers. *Proc. Natl. Acad. Sci. U.S.A.* **2005**, *102*, 3540–3545.
28. de la Torre, G.; Giacalone, F.; Segura, J. L.; Martín, N.; Guldi, D. M. Electronic Communication through π-Conjugated Wires in Covalently Linked Porphyrin/C_{60} Ensembles. *Chem.—Eur. J.* **2005**, *11*, 1267–1280.
29. Imahori, H.; Fukuzumi, S. Porphyrin- and Fullerene-Based Molecular Photovoltaic Devices. *Adv. Funct. Mater.* **2004**, *14*, 525–536.
30. Imahori, H. Porphyrin-Fullerene Linked Systems as Artificial Photosynthetic Mimics. *Org. Biomol. Chem.* **2004**, *2*, 1425–1433.
31. Guldi, D. M.; Rahman, G. M. A.; Sgobba, V.; Ehli, C. Multifunctional Molecular Carbon Materials—From Fullerenes to Carbon Nanotubes. *Chem. Soc. Rev.* **2006**, *35*, 471–487.
32. Guldi, D. M. Nanometer Scale Carbon Structures for Charge-Transfer Systems and Photovoltaic Applications. *Phys. Chem. Chem. Phys.* **2007**, *9*, 1400–1420.
33. Vail, S. A.; *et al.* Energy and Electron Transfer in β-Alkynyl-Linked Porphyrin-[60]Fullerene Dyads. *J. Phys. Chem. B* **2006**, *110*, 14155–14166.
34. Kobori, Y.; Yamauchi, S.; Akiyama, K.; Tero-Kubota, S.; Imahori, H.; Fukuzumi, S.; Norris, J. R., Jr. Primary Charge-Recombination in an Artificial Photosynthetic Reaction Center. *Proc. Natl. Acad. Sci. U.S.A.* **2005**, *102*, 10017–10022.
35. Smitha, M. A.; Gopidas, K. R. Temperature Dependence of Photoinduced Electron Transfer in Hydrogen-Bonded Donor−Acceptor Systems. *Chem. Phys. Lett.* **2001**, *350*, 86–92.
36. Oswald, F.; Shafiqul Islam, D.-M.; Araki, Y.; Troiani, V.; Caballero, R.; de la Cruz, P.; Ito, O.; Langa, F. High Effectiveness of Oligothienylenevinylene as Molecular Wires in Zn-Porphyrin and C_{60} Connected Systems. *Chem. Commun.* **2007**, 4498–4500.
37. Santos, J.; Illescas, B. M.; Wielopolski, M.; Silva, A. M. G.; Tome, A. C.; Guldi, D. M.; Martín, N. Efficient Electron Transfer in β-Substituted Porphyrin-C_{60} Dyads Connected through a *p*-Phenylenevinylene Dimer. *Tetrahedron* **2008**, *64*, 11404–11408.
38. Adler, A. D.; Longo, F. R.; Finarelli, J. D.; Goldmacher, J.; Assour, J.; Korsakoff, L. A Simplified Synthesis for *meso*-Tetraphenylporphine. *J. Org. Chem.* **1967**, *32*, 476.
39. van der Pol, C.; Bryce, M. R.; Wielopolski, M.; Atienza-Castellanos, C.; Guldi, D. M.; Fillipone, S.; Martín, N. Energy Transfer in Oligofluorene-C_{60} and C_{60}-Oligofluorene-C_{60} Donor−Acceptor Conjugates. *J. Org. Chem.* **2007**, *72*, 6662–6671.
40. Prato, M.; Maggini, M. Fulleropyrrolidines: A Family of Full-Fledged Fullerene Derivatives. *Acc. Chem. Res.* **1998**, *31*, 519–526.
41. Maggini, M.; Scorrano, G.; Prato, M. Addition of Azomethine Ylides to C_{60}: Synthesis, Characterization, and Functionalization of Fullerene Pyrrolidines. *J. Am. Chem. Soc.* **1993**, *115*, 9798–9799.
42. Haufler, R. E.; *et al.* Efficient Production of C_{60} (Buckminsterfullerene), $C_{60}H_{36}$, and the Solvated Buckide Ion. *J. Phys. Chem.* **1990**, *94*, 8634–8636.
43. Allemand, P. M.; Koch, A.; Wudl, F.; Rubin, Y.; Diederich, F.; Alvarez, M. M.; Anz, S. J.; Whetten, R. L. Two Different Fullerenes Have the Same Cyclic Voltammetry. *J. Am. Chem. Soc.* **1991**, *113*, 1050–1051.
44. Echegoyen, L.; Echegoyen, L. E. Electrochemistry of Fullerenes and Their Derivatives. *Acc. Chem. Res.* **1998**, *31*, 593–601.
45. Dewar, M. J. S.; Zoebisch, E. G.; Healy, E. F.; Stewart, J. J. P. Development and Use of Quantum Mechanical Molecular Models. AM1: A New General Purpose Quantum Mechanical Molecular Model. *J. Am. Chem. Soc.* **1985**, *107*, 3902–3909.
46. Guldi, D. M.; Prato, M. Excited-State Properties of C_{60} Fullerene Derivatives. *Acc. Chem. Res.* **2000**, *33*, 695–703.
47. Williams, A. T. R.; Winfield, S. A.; Miller, J. N. Relative Fluorescence Quantum Yields Using a Computer-Controlled Luminescence Spectrometer. *Analyst* **1983**, *108*, 1067–1071.
48. Brun, A. M.; Harriman, A.; Heitz, V.; Sauvage, J.-P. Charge Transfer across Oblique Bisporphyrins: Two-Center Photoactive Molecules. *J. Am. Chem. Soc.* **1991**, *113*, 8657–8663, and references therein.
49. Rodriguez, J.; Kirmaier, C.; Holten, D. Optical Properties of Metalloporphyrin Excited States. *J. Am. Chem. Soc.* **1989**, *111*, 6500–6506.
50. Guldi, D. M. Fullerene-Porphyrin Architectures; Photosynthetic Antenna and Reaction Center Models. *Chem. Soc. Rev.* **2002**, *31*, 22–36.
51. Note, the presence of a distinct band at 840 nm for the compounds with the longest oFL bridges, *i.e.*, **3b** and **4b**, which corresponds to the ZnP triplet excited-state signature. The moderate electron-transfer rate constant in **3b** and **4b** (2.4×10^8 and 7×10^7 s^{-1} in THF, respectively) lead, together with the large distance between donor and acceptor, to render the intersystem crossing process feasible as a deactivation pathway (Figure 10). As confirmed by molecular modeling, the energy of the charge-separated state is raised upon increasing the distance between donor and acceptor due to the linearly increasing change of dipole moments ΔD.
52. Martin, N.; Giacalone, F.; Segura, J. L.; Guldi, D. M. Mimicking Photosynthesis: Covalent [60]Fullerene-Based Donor−Acceptor Ensembles. *Synth. Met.* **2004**, *147*, 57–61.